Gauge invariance and hyperforce correlation theory for equilibrium fluid mixtures

Joshua Matthes*,[1] Silas Robitschko*,[1] Johanna Müller,[1]
Sophie Hermann,[2] Florian Sammüller,[1] and Matthias Schmidt[1]

[1]*Theoretische Physik II, Physikalisches Institut, Universität Bayreuth, D-95447 Bayreuth, Germany*
[2]*CNRS, Sorbonne Université, Physicochimie des Electrolytes et Nanosystèmes Interfaciaux, F-75005 Paris, France.*
(Dated: 23 September 2025)

We formulate gauge invariance for the equilibrium statistical mechanics of classical multi-component systems. Species-resolved phase space shifting constitutes a gauge transformation which we analyze using Noether's theorem and shifting differential operators that encapsulate the gauge invariance. The approach yields exact equilibrium sum rules for general mixtures. Species-resolved gauge correlation functions for the force-force and force-gradient pair correlation structure emerge on the two-body level. Exact 3g-sum rules relate these correlation functions to the spatial Hessian of the partial pair distribution functions. General observables are associated with hyperforce densities that measure the covariance of the given observable with the interparticle, external, and diffusive partial force density observables. Exact hyperforce and Lie algebra sum rules interrelate these correlation functions with each other. The practical accessibility of the framework is demonstrated for binary Lennard-Jones mixtures using both adaptive Brownian dynamics and grand canonical Monte Carlo simulations. Specifically, we investigate the force-force pair correlation structure of the Kob-Andersen bulk liquid and we show results for representative hyperforce correlation functions in Wilding *et al.*'s symmetrical mixture confined between two asymmetric planar parallel walls.

I. INTRODUCTION

Soft matter consists naturally of several different microscopic components [1, 2], with ions in electrolytes [3–10] and differently-sized colloids in glass forming mixtures being prominent examples for the diverse range of systems that display a wide variety of physical effects. Targeting specific phenomena often requires bespoke treatment. In particular the glass formation phenomenon has been studied on the basis of a plethora of order parameters, including the use of machine learning [11, 12] and analyzing structural motifs [13]. A common observation in this realm is the similarity of the liquid and glass states when analyzed on the pair correlation level, as expressed succinctly by the authors of Ref. [14] who note that "structural changes appear to be minor when looking at two-point measures like the structure factor, [while] higher-order measures reveal a richer behavior". A comparison of results for pair distribution functions of different microscopic glass forming models is presented in Ref. [12]. Going beyond the pair distribution function, and its species-labelled generalization to *partial* pair distribution functions that characterize mixtures, is often useful.

Noether's theorem [15, 16] was applied in a variety of different settings in statistical physics [17–23]. The theorem provides the basis for the recent thermal invariance theory [24–36]. This approach is based on a rigorous invariance of equilibrium averages and of thermodynamic potentials against specific shifting and rotation operations, as described below in detail. Force and torque correlation functions emerge systematically within the

framework and these are interrelated by exact statistical mechanical identities ("sum rules"). The sum rules take on the role that conservation laws play in conventional uses of the Noether theorem, where typically the invariances within a dynamical description are analysed.

The statistical mechanical gauge invariance gives rise to force-force and force-gradient two-body correlation functions that reveal much insight into the bulk structure of liquids and more general soft matter systems [29, 30]. Thereby the spatially resolved force-force correlation function is crucial and distinct from the temporal force autocorrelation function of tagged particle motion [37], see e.g. Ref. [38] for a study of the effects of shear. Here the force-force correlation function rather measures the covariance of the forces that act on each particle in an interacting pair. Similarly, the force-gradient correlation function represents the mean gradient of the force that acts on one of the particles upon displacing the second particle. The quantitative analysis of these gauge correlation functions allows one to trace a broad range of microscopic structuring effects, from clear signatures of interparticle attraction to chain formation in gels and orientational order in liquid crystals [29, 30].

The theoretical structure emerges from an inherent gauge invariance of statistical mechanics against phase space shifting [32–34]. Popular accounts have been given [35, 36] and a dynamical generalization was presented very recently [34]. Statistical mechanical sum rules were shown to play an important practical role in assessing the quality of neural functionals obtained with simulation-based supervised machine learning [39–50]. That the machine-learning approach entails significant potential for carrying out efficient computational work was demonstrated in the study of charged systems [6–10] on the basis of classical density functional theory [51].

---

*Authors contributed equally.

Here we present the generalization of the gauge correlation framework [24–34] to multi-component systems in thermal equilibrium. The emerging species-resolved forms of the sum rules possess similar mathematical form as in the analogous one-component case. The species-resolved sum rules carry species labels in a systematic way. The relative simplicity is important for the practical applications in both theoretical and simulation work. As a representative model, we consider the iconic binary Lennard-Jones fluid [2], which is a popular starting point for investigating complex (fluid) bulk phase behaviour and associated interfacial wetting phenomena [52–61]. A particular symmetrical parameterization investigated by Wilding *et al.* [55–61] provides a simple case that features only a single common lengthscale. Furthermore we consider the popular Kob-Andersen model [62, 63] as a prototypical asymmetrical binary mixture. Recent work was addressed at its phase diagram [64] and locally favoured structures [65], devitrification processes [66], a crystallization instability [67], many-body correlations [68], ultrastability [69], and aging [70].

The paper is organized as follows. In Sec. II we present the species-resolved gauge theory, including the description of the microscopic model Hamiltonian (Sec. II A), the thermal ensemble (Sec. II B), the sum rules that emerge from invariance against species-resolved phase space shifting (Sec. II C), and the gauge invariance for statistical mechanical microstates (Sec. II D). In Sec. III we describe the sum rules for the force-force and force gradient correlation functions in general inhomogeneous situations (Sec. III A), the reduction to species-resolved '3g-sum rules' for bulk states (Sec. III B), and exact global and local identities (Sec. III C). We present the hyperforce correlation theory for mixtures in Sec. IV, including the general locally-resolved framework for general observables (Sec. IV A), the associated global sum rules (Sec. IV B), and the application to several specific choices both within the locally-resolved (Sec. IV C) and the global (Sec. IV D) cases. In Sec. V we present our simulation results for the bulk force-force correlation structure of the Kob-Andersen liquid (Sec. V A) and for the confined symmetric Lennard-Jones system (Sec. V B). In Sec. VI we present our conclusions and give an outlook on possible future work.

II. SHIFTING GAUGE TRANSFORMATION

A. Microscopic multi-component model

We consider systems with M distinct species of particles. Each species $\alpha = 1, \ldots, M$ consists of N_α particles that possess identical properties. To implement the book-keeping of the different components, we group all particle indices i that constitute the species α together into an index set $\mathcal{N}_\alpha$. Summing over all particles of species α can then be written succinctly as $\sum_{i \in \mathcal{N}_\alpha}$. Further summation over all species is expressed as the sum $\sum_\alpha$, where the summation index α runs over all species $1, \ldots, M$. An example for this mechanism is the total number of particles $N = \sum_\alpha N_\alpha$. As a special (and admittedly extreme) case, this labelling allows one to address all particles individually, via setting $M = N$ and $N_\alpha = 1$ for all α. Each index set then contains a single element, $\mathcal{N}_\alpha = \{\alpha\}$, and the sum over particles of this species collapses to the single contribution $\alpha = i$, hence effectively rendering α the particle index.

The microscopic model in d spatial dimensions is described on the basis of its position coordinates $\mathbf{r}_1, \ldots, \mathbf{r}_N \equiv \mathbf{r}^N$ and the linear momenta $\mathbf{p}_1, \ldots, \mathbf{p}_N \equiv \mathbf{p}^N$. The Hamiltonian H contains kinetic, interparticle, and external energy contributions according to the following standard form:

$$H = \sum_\alpha \sum_{i \in \mathcal{N}_\alpha} \frac{\mathbf{p}_i^2}{2m_\alpha} + u(\mathbf{r}^N) + \sum_\alpha \sum_{i \in \mathcal{N}_\alpha} V_{\text{ext}}^{(\alpha)}(\mathbf{r}_i), \quad (1)$$

where m_α denotes the mass of particles of species α, $u(\mathbf{r}^N)$ is the interparticle interaction potential, and the one-body external potential $V_{\text{ext}}^{(\alpha)}(\mathbf{r})$ acts on species α at position $\mathbf{r}$. That different particles of the same species behave in the same way is encoded in the permutation symmetry of the interparticle interaction potential $u(\mathbf{r}^N)$ such that the value of $u(\mathbf{r}^N)$ remains unchanged upon interchanging the positions of two particles of the same species. A common form of $u(\mathbf{r}^N)$ is generated by pair potentials $\phi_{\alpha\alpha'}(r)$ that act between two particles of species α and α' that are separated by a center-center distance r. The total interparticle potential can then be written explicitly as $u(\mathbf{r}^N) = \sum_\alpha \sum_{\alpha'} \sum_{i \in \mathcal{N}_\alpha} \sum'_{j \in \mathcal{N}_{\alpha'}} \phi_{\alpha\alpha'}(|\mathbf{r}_i - \mathbf{r}_j|)/2$, where the primed sum indicates that the case $i = j$ has been omitted, the factor $1/2$ corrects for double counting, the species-swap symmetry $\phi_{\alpha\alpha'}(r) = \phi_{\alpha'\alpha}(r)$ is implied, and the sums over particle indices α and α' each run over all species $1, \ldots, M$.

B. Equilibrium ensemble and one-body observables

The statistical mechanics of the mixture is formulated in the standard way and we work specifically in the grand ensemble. Formally analogous derivations in the canonical ensemble yield, for fixed number of particles, sum rules that are identical in form to the grand canonical versions. We exemplify explicitly below in Sec. V the validity both with adaptive Brownian dynamics, as representing the canonical ensemble, as well as with grand canonical Monte Carlo simulations, as representing the coupling to a particle bath.

At temperature T and species-resolved chemical potentials $\mu_1, \ldots, \mu_M$ the grand potential Ω and the grand partition sum Ξ are given respectively by

$$\Omega = -k_B T \ln \Xi, \quad (2)$$

$$\Xi = \text{Tr} \, e^{-\beta(H - \sum_\alpha \mu_\alpha N_\alpha)}, \quad (3)$$

where k_B denotes the Boltzmann constant and $\beta = 1/(k_BT)$. The classical trace operation in the grand ensemble is given by $\text{Tr}\cdot = \sum_{N_1}\ldots\sum_{N_M}(N_1!\ldots N_M!h^{dN})^{-1}\int d\mathbf{r}^N\int d\mathbf{p}^N\cdot$, where the sums over particle numbers $N_1,\ldots,N_M$ each range from 0 to ∞, the symbol h indicates the Planck constant, and the phase space integral is abbreviated as $\int d\mathbf{r}^N\int d\mathbf{p}^N\cdot = \int d\mathbf{r}_1\ldots d\mathbf{r}_N\int d\mathbf{p}_1\ldots d\mathbf{p}_N\cdot\cdot$. The corresponding grand ensemble probability distribution (Gibbs measure) is

$$\Psi = e^{-\beta(H-\sum_\alpha \mu_\alpha N_\alpha)}/\Xi, \tag{4}$$

where the normalization factor Ξ is the grand partition sum (3) and thermal averages can then be written in the compact form $\langle\cdot\rangle = \text{Tr}\cdot\Psi$.

We give a summary of several relevant averages that characterize the mixture. The partial density profile $\rho_\alpha(\mathbf{r})$ of species α is the average of the corresponding one-body density "operator" (phase space function), $\rho_\alpha(\mathbf{r}) = \langle\hat{\rho}_\alpha(\mathbf{r})\rangle$, where the microscopic density observable of species α is given as $\hat{\rho}_\alpha(\mathbf{r}) = \sum_{i\in\mathcal{N}_\alpha}\delta(\mathbf{r}-\mathbf{r}_i)$, with $\delta(\cdot)$ denoting the Dirac distribution. Correspondingly, the mean interparticle force density that acts on species α is $\mathbf{F}_{\text{int}}^{(\alpha)}(\mathbf{r}) = \langle\hat{\mathbf{F}}_{\text{int}}^{(\alpha)}(\mathbf{r})\rangle$, where the species-resolved interparticle force density observable is defined as

$$\hat{\mathbf{F}}_{\text{int}}^{(\alpha)}(\mathbf{r}) = -\sum_{i\in\mathcal{N}_\alpha}\delta(\mathbf{r}-\mathbf{r}_i)\nabla_i u(\mathbf{r}^N), \tag{5}$$

where ∇_i denotes the derivative with respect to $\mathbf{r}_i$. Similarly, the species-resolved average kinetic stress is $\boldsymbol{\tau}_\alpha(\mathbf{r}) = \langle\hat{\boldsymbol{\tau}}_\alpha(\mathbf{r})\rangle$, with the kinetic stress observable being defined as

$$\hat{\boldsymbol{\tau}}_\alpha(\mathbf{r}) = -\sum_{i\in\mathcal{N}_\alpha}\delta(\mathbf{r}-\mathbf{r}_i)\frac{\mathbf{p}_i\mathbf{p}_i}{m_\alpha}, \tag{6}$$

where $\mathbf{p}_i\mathbf{p}_i$ indicates the dyadic product of the momentum of particle i with itself. These observables can be combined into a species-resolved total force operator (phase space function), given as

$$\hat{\mathbf{F}}_\alpha(\mathbf{r}) = \nabla\cdot\hat{\boldsymbol{\tau}}_\alpha(\mathbf{r}) + \hat{\mathbf{F}}_U^{(\alpha)}(\mathbf{r}), \tag{7}$$

where ∇ denotes the derivative with respect to $\mathbf{r}$, and the potential force density observable for species α is $\hat{\mathbf{F}}_U^{(\alpha)}(\mathbf{r}) = \hat{\mathbf{F}}_{\text{int}}^{(\alpha)}(\mathbf{r}) - \hat{\rho}_\alpha(\mathbf{r})\nabla V_{\text{ext}}^{(\alpha)}(\mathbf{r})$. The averaged total force density acting on species α then follows as the average $\mathbf{F}_\alpha(\mathbf{r}) = \langle\hat{\mathbf{F}}_\alpha(\mathbf{r})\rangle$. The species-resolved potential-only force density is $\mathbf{F}_U^{(\alpha)}(\mathbf{r}) = \langle\hat{\mathbf{F}}_U^{(\alpha)}(\mathbf{r})\rangle$.

C. Species-resolved phase space shifting

In order to identify the thermal invariance of the mixture, we introduce shifting fields that are unique for each component α of the mixture, in generalization of the local

shifting transformation for pure systems [27–33]. Specifically, the species-resolved transformations are:

$$\mathbf{r}_i \to \mathbf{r}_i + \boldsymbol{\epsilon}_\alpha(\mathbf{r}_i), \tag{8}$$

$$\mathbf{p}_i \to [\mathbb{1} + \nabla_i\boldsymbol{\epsilon}_\alpha(\mathbf{r}_i)]^{-1}\cdot\mathbf{p}_i, \tag{9}$$

where particle i is of type α such that $i\in\mathcal{N}_\alpha$ and $\boldsymbol{\epsilon}_\alpha(\mathbf{r})$ is the d-dimensional vector field that displaces particles of component α. In Eq. (9) the symbol $\mathbb{1}$ denotes the $d\times d$-unit matrix, ∇_i is the derivative with respect to $\mathbf{r}_i$, and matrix inversion is indicated by the superscript -1. The transformations (8) and (9) retain the canonical properties of the one-component version [27–30], as the latter already acts merely individually on the position and the momentum of each particle i.

The generalized transformation (8) and (9) allows one to address the individual species separately. The strategy of the subsequent argumentation carries over straightforwardly from the one-component case [27–30], as we lay out in the following. The invariance of the grand potential implies $\Omega[\{\boldsymbol{\epsilon}_{\alpha'}\}] = \Omega$, where on the right hand side Ω with no argument is, as before, the grand potential (2) expressed in the original phase space variables. On the left hand side $\{\boldsymbol{\epsilon}_{\alpha'}\}$ indicates the set of all displacement fields $\{\boldsymbol{\epsilon}_1(\mathbf{r}),\ldots,\boldsymbol{\epsilon}_M(\mathbf{r})\}$, which are used to transform the phase space variables.

We consider invariance at first order in the displacement fields and follow the arguments for the one-component case [27–30], which allow one to conclude that $\delta\Omega[\{\boldsymbol{\epsilon}_{\alpha'}\}]/\delta\boldsymbol{\epsilon}_\alpha(\mathbf{r}) = 0$. Explicitly carrying out the functional derivative gives the following exact species-resolved force density balance:

$$-k_BT\nabla\rho_\alpha(\mathbf{r}) + \mathbf{F}_{\text{int}}^{(\alpha)}(\mathbf{r}) - \rho_\alpha(\mathbf{r})\nabla V_{\text{ext}}^{(\alpha)}(\mathbf{r}) = 0. \tag{10}$$

The derivation of Eq. (10) rests on the following operator identity, which is obtained from expressing the Hamiltonian (1) in the new coordinates such that it carries an apparent functional dependence on the set of shifting fields,

$$-\frac{\delta H[\{\boldsymbol{\epsilon}_{\alpha'}\}]}{\delta\boldsymbol{\epsilon}_\alpha(\mathbf{r})}\bigg|_{\{\boldsymbol{\epsilon}_{\alpha'}=0\}} = \hat{\mathbf{F}}_\alpha(\mathbf{r}). \tag{11}$$

The right hand side of Eq. (11) consists of the kinetic, interparticle, and external force densities described in Sec. II B. The thermal average of $\hat{\mathbf{F}}_\alpha(\mathbf{r})$ is generated via applying the functional derivative to the grand potential Ω, see its definition (2). These steps lead to Eq. (10), which can be written in more compact form as

$$\mathbf{F}_\alpha(\mathbf{r}) = 0. \tag{12}$$

For details about specific steps we refer the Reader to the description of the one-component case in Ref. [30].

D. Statistical mechanical gauge invariance

For the case of one-component systems, $M = 1$, the phase space variable transformation (8) and (9) was

shown to constitute a gauge transformation of the statistical mechanical microstates [32, 33]. Even though the microstates are transformed, any equilibrium average remains invariant under the transformation. In particular the phase space shifting is shown to be closely associated with a specific differential operator structure on phase space. These "shifting differential operators" apply to general phase space functions and they perform a role analogous to that of the explicit coordinate transformation (8) and (9). Here we generalize the statistical mechanical gauge invariance concept to mixtures and thus define the following species- and position-resolved phase space differential operators:

$$\boldsymbol{\sigma}_\alpha(\mathbf{r}) = \sum_{i\in\mathcal{N}_\alpha} [\delta(\mathbf{r}-\mathbf{r}_i)\nabla_i + \mathbf{p}_i\nabla\delta(\mathbf{r}-\mathbf{r}_i)\cdot\nabla_{\mathbf{p}_i}], \quad (13)$$

where $\nabla_{\mathbf{p}_i}$ denotes the derivative with respect to $\mathbf{p}_i$ and $\mathbf{p}_i\nabla$ is a dyadic product [32, 33]. The crucial difference to the one-component version $\boldsymbol{\sigma}(\mathbf{r})$ [32, 33] is the mere restriction of particle summation from a sum over all particles to $\sum_{i\in\mathcal{N}_\alpha}$ in Eq. (13).

The operators (13) are anti-self-adjoint on phase space and they satisfy nontrivial commutator structure, as respectively expressed by

$$\boldsymbol{\sigma}_\alpha^\dagger(\mathbf{r}) = -\boldsymbol{\sigma}_\alpha(\mathbf{r}), \quad (14)$$

$$[\boldsymbol{\sigma}_\alpha(\mathbf{r}), \boldsymbol{\sigma}_{\alpha'}(\mathbf{r}')] = \delta_{\alpha\alpha'}\boldsymbol{\sigma}_\alpha(\mathbf{r}')[\nabla\delta(\mathbf{r}-\mathbf{r}')]$$
$$+ \delta_{\alpha\alpha'}[\nabla\delta(\mathbf{r}-\mathbf{r}')]\boldsymbol{\sigma}_\alpha(\mathbf{r}), \quad (15)$$

where $\delta_{\alpha\alpha'}$ denotes the Kronecker symbol and the dagger indicates the adjoint, which for an operator $\mathcal{O}$ and two general phase space functions $\hat{A}(\mathbf{r}^N, \mathbf{p}^N)$ and $\hat{B}(\mathbf{r}^N, \mathbf{p}^N)$ is defined in the standard way via $\int d\mathbf{r}^N d\mathbf{p}^N \hat{A}\mathcal{O}\hat{B} = \int d\mathbf{r}^N d\mathbf{p}^N \hat{B}\mathcal{O}^\dagger\hat{A}$.

The localized shifting operators (13) can be combined together with their respective shifting fields $\boldsymbol{\epsilon}_\alpha(\mathbf{r})$, which play the role of gauge functions, to define integrated shifting operators

$$\Sigma[\{\boldsymbol{\epsilon}_\alpha\}] = \sum_\alpha \int d\mathbf{r}\boldsymbol{\epsilon}_\alpha(\mathbf{r})\cdot\boldsymbol{\sigma}_\alpha(\mathbf{r}), \quad (16)$$

where on the left hand side the bracketed argument indicates the functional dependence on the set of shifting fields $\{\boldsymbol{\epsilon}_1(\mathbf{r}), \ldots, \boldsymbol{\epsilon}_M(\mathbf{r})\}$. A given phase space function $\hat{A}(\mathbf{r}^N, \mathbf{p}^N)$ is then affected by the transformation to lowest order in the shifting fields and their spatial gradients as

$$\hat{A}(\tilde{\mathbf{r}}^N, \tilde{\mathbf{p}}^N) = \hat{A}(\mathbf{r}^N, \mathbf{p}^N) + \Sigma[\{\boldsymbol{\epsilon}_\alpha\}]\hat{A}(\mathbf{r}^N, \mathbf{p}^N), \quad (17)$$

where the tilde indicates the new phase space variables (8) and (9). The operators $\Sigma[\{\boldsymbol{\epsilon}_\alpha\}]$ satisfy nontrivial Lie algebra structure, such that the commutator is $[\Sigma[\{\boldsymbol{\epsilon}_\alpha\}], \Sigma[\{\boldsymbol{\epsilon}_\alpha'\}]] = \Sigma[\{\boldsymbol{\epsilon}_\alpha''(\mathbf{r})\}]$, where the difference shifting field is given by $\boldsymbol{\epsilon}_\alpha''(\mathbf{r}) = \boldsymbol{\epsilon}_\alpha(\mathbf{r})\cdot[\nabla\boldsymbol{\epsilon}_\alpha'(\mathbf{r})] - \boldsymbol{\epsilon}_\alpha'(\mathbf{r})\cdot[\nabla\boldsymbol{\epsilon}_\alpha(\mathbf{r})]$. Hence the integrated shifting operators

$\Sigma[\{\boldsymbol{\epsilon}_\alpha\}]$ continue to satisfy the Lie algebra structure described in Ref. [32], including the Jacobi identity.

Applying the localized shifting operators (13) to a given phase space function $\hat{A}(\mathbf{r}^N, \mathbf{p}^N)$ is identical to carrying out the following functional differentiation operations at first order:

$$\boldsymbol{\sigma}_\alpha(\mathbf{r})\hat{A} = \frac{\delta\hat{A}(\tilde{\mathbf{r}}^N, \tilde{\mathbf{p}}^N)}{\delta\boldsymbol{\epsilon}_\alpha(\mathbf{r})}\bigg|_{\{\boldsymbol{\epsilon}_\alpha=0\}}, \quad (18)$$

and at second order:

$$\boldsymbol{\sigma}_\alpha(\mathbf{r})\boldsymbol{\sigma}_{\alpha'}(\mathbf{r}')\hat{A} = \frac{\delta^2\hat{A}(\tilde{\mathbf{r}}^N, \tilde{\mathbf{p}}^N)}{\delta\boldsymbol{\epsilon}_\alpha(\mathbf{r})\delta\boldsymbol{\epsilon}_{\alpha'}(\mathbf{r}')}\bigg|_{\{\boldsymbol{\epsilon}_\alpha=0\}}$$
$$+ \delta_{\alpha\alpha'}[\nabla\delta(\mathbf{r}-\mathbf{r}')]\boldsymbol{\sigma}_\alpha(\mathbf{r})\hat{A}(\mathbf{r}^N, \mathbf{p}^N). \quad (19)$$

The (phase space) arguments of $\hat{A}(\mathbf{r}^N, \mathbf{p}^N)$ are suppressed on the above left hand sides for brevity. As indicated in the notation on the right hand sides, all partial shifting fields $\boldsymbol{\epsilon}_\alpha(\mathbf{r})$ are set to zero after the functional derivatives have been taken.

When applied to a specific observable $\hat{A}$ the species-resolved hyperforce density is $\hat{\mathbf{S}}_A^{(\alpha)}(\mathbf{r}) = \boldsymbol{\sigma}_\alpha(\mathbf{r})\hat{A}$, see Eqs. (13) and (18). Explicitly the resulting phase space form of the species-resolved hyperforce density is

$$\hat{\mathbf{S}}_A^{(\alpha)}(\mathbf{r}) = \sum_{i\in\mathcal{N}_\alpha} [\delta(\mathbf{r}-\mathbf{r}_i)\nabla_i\hat{A} + \mathbf{p}_i\nabla\delta(\mathbf{r}-\mathbf{r}_i)\cdot\nabla_{\mathbf{p}_i}\hat{A}]. \quad (20)$$

From the commutator relationship (15) the following Lie sum rules are obtained upon phase space averaging:

$$\langle\hat{\mathbf{S}}_A^{(\alpha)}(\mathbf{r})\beta\hat{\mathbf{F}}_{\alpha'}(\mathbf{r}')\rangle - \langle\beta\hat{\mathbf{F}}_\alpha(\mathbf{r})\hat{\mathbf{S}}_A^{(\alpha')}(\mathbf{r}')\rangle$$
$$= \delta_{\alpha\alpha'}\{\mathbf{S}_A^{(\alpha)}(\mathbf{r}')[\nabla\delta(\mathbf{r}-\mathbf{r}')] + [\nabla\delta(\mathbf{r}-\mathbf{r}')]\mathbf{S}_A^{(\alpha)}(\mathbf{r})\}. \quad (21)$$

As a special case, when the right hand side of (21) vanishes, we have:

$$\langle\hat{\mathbf{S}}_A^{(\alpha)}(\mathbf{r})\hat{\mathbf{F}}_{\alpha'}(\mathbf{r}')\rangle - \langle\hat{\mathbf{F}}_\alpha(\mathbf{r})\hat{\mathbf{S}}_A^{(\alpha')}(\mathbf{r}')\rangle = 0, \quad (22)$$

which holds true provided that $\alpha \neq \alpha'$ or $\mathbf{r} \neq \mathbf{r}'$.

We next describe several concrete consequences of the gauge invariance for the correlation structure of soft matter mixtures.

III. FORCE CORRELATION FUNCTIONS

A. Inhomogeneous partial pair force correlations

Addressing second-order phase space shifting, we consider the functional Hessian with respect to the shifting fields, i.e. the species-resolved second derivatives

$\delta^2\Omega[\{\boldsymbol{\epsilon}_{\alpha''}\}]/\delta\boldsymbol{\epsilon}_\alpha(\mathbf{r})\delta\boldsymbol{\epsilon}_{\alpha'}(\mathbf{r}') = 0$. One finds upon carrying out the explicit calculation on the basis of Eq. (11) the following result:

$$\beta\langle\hat{\mathbf{F}}_\alpha(\mathbf{r})\hat{\mathbf{F}}_{\alpha'}(\mathbf{r}')\rangle = \left\langle\frac{\delta^2 H[\{\boldsymbol{\epsilon}_{\alpha''}\}]}{\delta\boldsymbol{\epsilon}_\alpha(\mathbf{r})\delta\boldsymbol{\epsilon}_{\alpha'}(\mathbf{r}')}\right\rangle\Bigg|_{\{\boldsymbol{\epsilon}_{\alpha''}=0\}}, \quad (23)$$

where again the shifting fields are set to zero after the functional derivatives of the Hamiltonian have been taken. We recall that $\hat{\mathbf{F}}_\alpha(\mathbf{r})$ indicates the species- and position-resolved total force density observable (7), which includes the potential forces and the divergence of the kinetic stress contribution. The sum rule (23) generalizes the corresponding one-component identity [29, 30]. It is useful to split off the potential forces in the sum rule (23) and to furthermore also discriminate between self and distinct cases according to whether the same or two different particles contribute to the occurring double sums. In the derivation one can make use of Eq. (19), setting $\hat{A} = H$ therein, and we refer to Ref. [30] for further details on the corresponding reasoning.

The resulting position-dependent two-body distinct sum rule has the following species-resolved form:

$$\langle\beta\hat{\mathbf{F}}_U^{(\alpha)}(\mathbf{r})\beta\hat{\mathbf{F}}_U^{(\alpha')}(\mathbf{r}')\rangle_{\text{dist}} = \nabla\nabla'\rho_2^{(\alpha\alpha')}(\mathbf{r},\mathbf{r}')$$
$$+ \left\langle\sum_{i\in\mathcal{N}_\alpha}\sum_{j\in\mathcal{N}_{\alpha'}}'\delta(\mathbf{r}-\mathbf{r}_i)\delta(\mathbf{r}'-\mathbf{r}_j)\nabla_i\nabla_j\beta u(\mathbf{r}^N)\right\rangle, \quad (24)$$

where the (distinct) two-body density is defined as the thermal average $\rho_2^{(\alpha\alpha')}(\mathbf{r},\mathbf{r}') = \langle\hat{\rho}_\alpha(\mathbf{r})\hat{\rho}_{\alpha'}(\mathbf{r}')\rangle_{\text{dist}} = \langle\sum_{i\in\mathcal{N}_\alpha}\sum_{j\in\mathcal{N}_{\alpha'}}'\delta(\mathbf{r}-\mathbf{r}_i)\delta(\mathbf{r}'-\mathbf{r}_j)\rangle$. We recall that the primed sum indicates the restriction $j\neq i$, which only plays a role for the case of identical species, $\alpha = \alpha'$. The distinct average on the left hand side of Eq. (24) correspondingly excludes the case $i = j$ in the occurring double sums over particles when writing out the two potential force operators.

The corresponding self part of the sum rule follows from considering double occurrences of the same particle in Eq. (23), which leads to the following exact identity:

$$\langle\beta\hat{\mathbf{F}}_U^{(\alpha)}(\mathbf{r})\beta\hat{\mathbf{F}}_U^{(\alpha)}(\mathbf{r})\rangle_{\text{self}} = \nabla\nabla\rho_\alpha(\mathbf{r})$$
$$+ \left\langle\sum_{i\in\mathcal{N}_\alpha}\delta(\mathbf{r}-\mathbf{r}_i)\nabla_i\nabla_i\beta u(\mathbf{r}^N)\right\rangle + \rho_\alpha(\mathbf{r})\nabla\nabla\beta V_{\text{ext}}^{(\alpha)}(\mathbf{r}). \quad (25)$$

The self part on the left hand side of Eq. (25) involves only the case of the same particle occurring twice in the double sum, such that this term constitutes the following dyadic product $\langle\beta^2\sum_{i\in\mathcal{N}_\alpha}\delta(\mathbf{r}-\mathbf{r}_i)[\nabla_i\hat{U}][\nabla_i\hat{U}]\rangle$, where $-\nabla_i\hat{U}(\mathbf{r}^N) = -\nabla_i[u(\mathbf{r}^N)+V_{\text{ext}}^{(\alpha)}(\mathbf{r}_i)]$ is the potential force that acts on particle i.

B. Bulk fluid 3g-sum rule for mixtures

We can simplify the above general two-body framework by resolving only the dependence on the relative distance between the two positions $\mathbf{r}$ and $\mathbf{r}'$. The standard partial (species-labelled) pair distribution function is given as

$$g_{\alpha\alpha'}(r) = \frac{\rho_2^{(\alpha\alpha')}(\mathbf{r},\mathbf{r}')}{\rho_\alpha^b\rho_{\alpha'}^b}, \quad (26)$$

where ρ_α^b indicates the bulk density of species α and the distance is $r = |\mathbf{r}-\mathbf{r}'|$. Analogously, the partial bulk force-force and force-gradient pair correlation functions are defined respectively as

$$\mathsf{g}_{ff}^{(\alpha\alpha')}(r) = \frac{\beta^2}{\rho_\alpha^b\rho_{\alpha'}^b}\langle\hat{\mathbf{F}}_{\text{int}}^{(\alpha)}(\mathbf{r})\hat{\mathbf{F}}_{\text{int}}^{(\alpha')}(\mathbf{r}')\rangle_{\text{dist}}, \quad (27)$$

$$\mathsf{g}_{\nabla f}^{(\alpha\alpha')}(r) =$$
$$-\frac{\beta}{\rho_\alpha^b\rho_{\alpha'}^b}\left\langle\sum_{i\in\mathcal{N}_\alpha}\sum_{j\in\mathcal{N}_{\alpha'}}'\delta(\mathbf{r}-\mathbf{r}_i)\delta(\mathbf{r}'-\mathbf{r}_j)\nabla_i\nabla_j u(\mathbf{r}^N)\right\rangle. \quad (28)$$

For a bulk mixture, where $V_{\text{ext}}^{(\alpha)}(\mathbf{r}) = 0$ for all α, we can simplify the inhomogeneous force correlation sum rule Eq. (24) to obtain the following homogeneous form:

$$\nabla\nabla g_{\alpha\alpha'}(r) + \mathsf{g}_{\nabla f}^{(\alpha\alpha')}(r) + \mathsf{g}_{ff}^{(\alpha\alpha')}(r) = 0, \quad (29)$$

which reduces to the one-component 3g-sum rule $\nabla\nabla g(r)+\mathsf{g}_{\nabla f}(r)+\mathsf{g}_{ff}(r) = 0$ in the case of single species [29, 30]. We have generalized the three pair correlation functions via restriction of the sums over all particles to sums over the appropriate index sets. Furthermore we have replaced the normalization factor ρ_b^2 by $\rho_\alpha^b\rho_{\alpha'}^b$, where the bulk number density of species α is $\rho_\alpha^b = \langle N_\alpha\rangle/V$; we recall that N_α is the number of particles of species α, and V indicates the system volume.

As in the one-component case [29, 30], the two nontrivial spatial components of the tensorial identity (29) are parallel ($\|$) and perpendicular ($\perp$) to the distance vector between the two particles and hence

$$g_{\alpha\alpha'}''(r) + g_{\nabla f\|}^{(\alpha\alpha')}(r) + g_{ff\|}^{(\alpha\alpha')}(r) = 0, \quad (30)$$

$$\frac{g_{\alpha\alpha'}'(r)}{r} + g_{\nabla f\perp}^{(\alpha\alpha')}(r) + g_{ff\perp}^{(\alpha\alpha')}(r) = 0, \quad (31)$$

where Eq. (31) holds for systems with spatial dimensionality $d \geq 2$. The primed functions in Eqs. (30) and (31) are derivatives by the argument, such that $g_{\alpha\alpha'}'(r)$ and $g_{\alpha\alpha'}''(r)$ are respectively the first and second derivatives of the partial pair distribution function $g_{\alpha\alpha'}(r)$ with respect to distance r.

For fluid mixtures where the particles interact solely via pair potentials $\phi_{\alpha\alpha'}(r)$, we have

$$\mathsf{g}_{\nabla f}^{(\alpha\alpha')}(r) = g_{\alpha\alpha'}(r)\beta\nabla\nabla\phi_{\alpha\alpha'}(r), \quad (32)$$
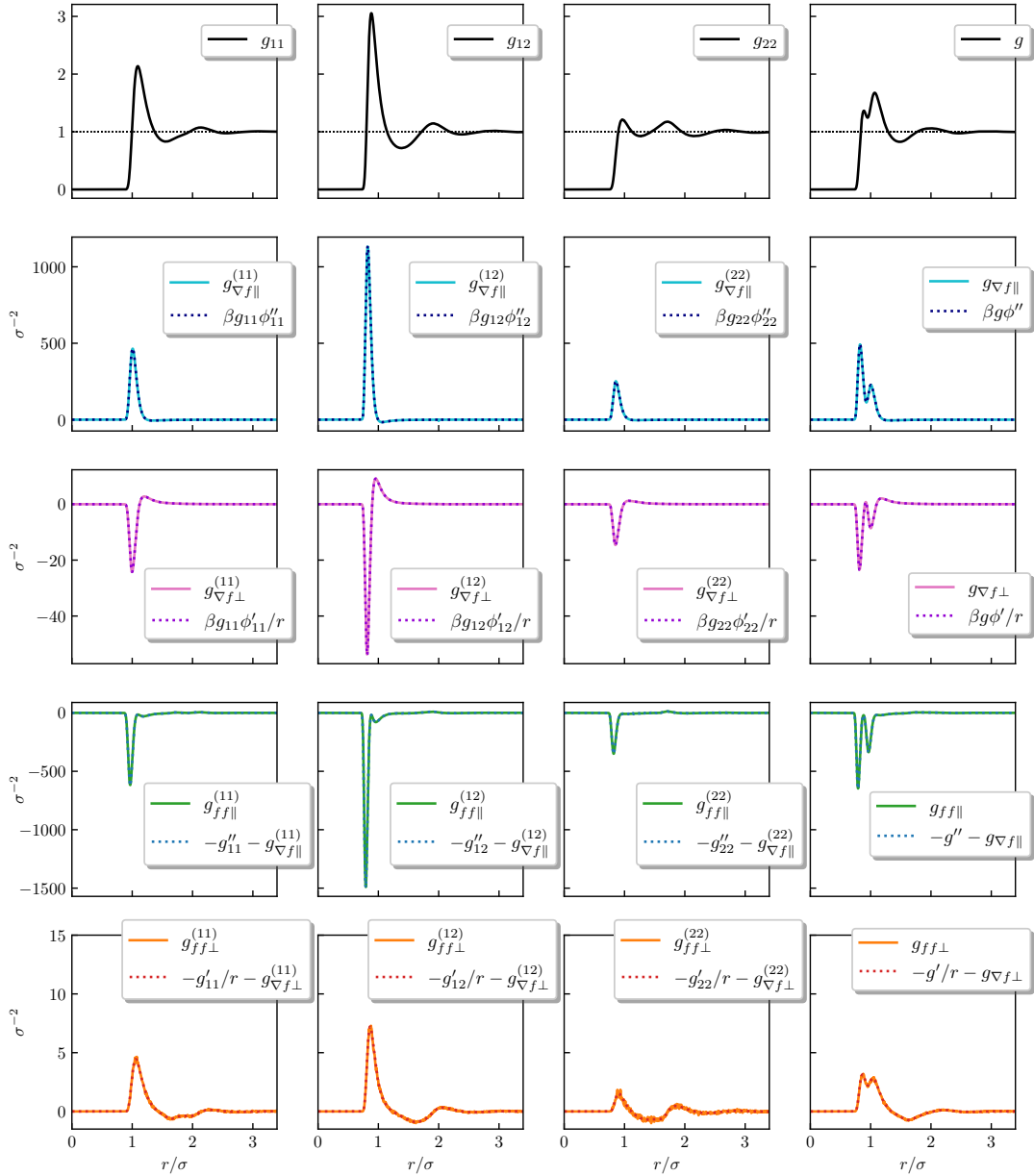
FIG. 1: Two-body gauge correlation functions of the Kob-Andersen liquid at reduced temperature $k_B T/\epsilon = 1.1$ and scaled partial bulk densities $\rho_1^b \sigma^3 = 0.591$ and $\rho_2^b \sigma^3 = 0.253$. Results are shown as a function of the scaled interparticle distance r/σ for species $\alpha\alpha' = 11$ (first column), 12 (second column), 22 (third column), and for the agglomerated quantities (fourth column). Top row: partial pair distribution functions $g_{\alpha\alpha'}(r)$. Second row: the parallel component of the force-gradient correlation function $g_{\nabla f\parallel}^{(\alpha\alpha')}(r)$ agrees numerically with $g_{\alpha\alpha'}(r)\beta\phi''_{\alpha\alpha'}(r)$, cf. Eq. (32). Third row: the corresponding perpendicular component $g_{\nabla f\perp}^{(\alpha\alpha')}(r)$ agrees numerically with $g_{\alpha\alpha'}(r)\beta\phi'_{\alpha\alpha'}(r)/r$, cf. Eq. (32). Fourth row: the parallel component of the force-force correlation function $g_{ff\parallel}^{(\alpha\alpha')}(r)$ agrees numerically with $-g''_{\alpha\alpha'}(r) - g_{\nabla f\parallel}^{(\alpha\alpha')}(r)$, as expected from the sum rules (30) (first to third panel) and (36) (last panel). Bottom row: the corresponding perpendicular component $g_{ff\perp}^{(\alpha\alpha')}(r)$ agrees numerically with $-g'_{\alpha\alpha'}(r)/r - g_{\nabla f\perp}^{(\alpha\alpha')}(r)$, as expected from sum rules (31) (first to third panels) and (37) (last panel).

where $\nabla\nabla\phi_{\alpha\alpha'}(r)$ possesses one nontrivial parallel component, $\phi''_{\alpha\alpha'}(r)$, and two identical perpendicular components, $\phi'_{\alpha\alpha'}(r)/r$. As a consequence, for such pairwise interacting mixtures we can express Eqs. (30) and (31) in the respective forms:

$$g''_{\alpha\alpha'}(r) + g_{\alpha\alpha'}(r)\beta\phi''_{\alpha\alpha'}(r) + g_{ff\parallel}^{(\alpha\alpha')}(r) = 0, \qquad (33)$$

$$\frac{g'_{\alpha\alpha'}(r)}{r} + g_{\alpha\alpha'}(r)\frac{\beta\phi'_{\alpha\alpha'}(r)}{r} + g_{ff\perp}^{(\alpha\alpha')}(r) = 0. \qquad (34)$$

All sum rules reduce to their one-component versions [30] in the limit of a single component. This also applies when considering 'agglomerated' correlation functions that ignore the species labelling, as we demonstrate in the following.

We introduce species-resolved concentration variables $c_\alpha = \rho_\alpha^b/\rho^b$ where the total bulk density is $\rho^b = \sum_\alpha \rho_\alpha^b$. Then summing over species yields the following 'colour-blind' or 'species-agnostic' versions as linear combinations of the species-resolved correlation functions. We obtain the agglomerated pair distribution function $g(r) = \sum_{\alpha,\alpha'} c_\alpha c_{\alpha'} g_{\alpha\alpha'}(r)$, the force-gradient correlation function $\mathbf{g}_{\nabla f}(r) = \sum_{\alpha,\alpha'} c_\alpha c_{\alpha'} \mathbf{g}_{\nabla f}^{(\alpha\alpha')}(r)$, which for pairwise interactions can be written as $\mathbf{g}_{\nabla f}^{(\alpha\alpha')}(r) = \sum_{\alpha\alpha'} c_\alpha c_{\alpha'} g_{\alpha\alpha'}(r)\nabla\nabla\beta\phi_{\alpha\alpha}(r)$, and the force-force correlation function $\mathbf{g}_{ff}(r) = \sum_{\alpha,\alpha'} c_\alpha c_{\alpha'} \mathbf{g}_{ff}^{(\alpha\alpha')}(r)$. Then the 3g-sum rule is obtained in the 'agglomerated' version:

$$\nabla\nabla g(r) + \mathbf{g}_{\nabla f}(r) + \mathbf{g}_{ff}(r) = 0, \tag{35}$$

which is formally identical to the single-component sum rule [29, 30]. The two relevant spatial tensor components are parallel and transversal to the interparticle distance vector and they satisfy respectively the following sum rules:

$$g''(r) + g_{\nabla f\parallel}(r) + g_{ff\parallel}(r) = 0, \tag{36}$$

$$\frac{g'(r)}{r} + g_{\nabla f\perp}(r) + g_{ff\perp}(r) = 0. \tag{37}$$

We present results from simulation work in Sec. V to demonstrate the accessibility of all partial two-body gauge correlation functions together with tests of the relevant sum rules that these satisfy.

C. Global and local two-body sum rules

We have so far treated position-resolved cases where the spatial dependence is retained. A global second order sum rule is obtained from either considering spatially constant displacements $\boldsymbol{\epsilon}_\alpha(\mathbf{r}) = \boldsymbol{\epsilon}_\alpha = \text{const}$ or alternatively integrating the spatially resolved identity (23) over both position variables and summing over both species. The result of both routes of derivation is the same and it is given by

$$\sum_{\alpha\alpha'} \int d\mathbf{r} d\mathbf{r}' H_2^{(\alpha\alpha')}(\mathbf{r},\mathbf{r}')\nabla V_{\text{ext}}^{(\alpha)}(\mathbf{r})\nabla' V_{\text{ext}}^{(\alpha')}(\mathbf{r}')$$
$$= k_B T \sum_\alpha \int d\mathbf{r}\rho_\alpha(\mathbf{r})\nabla\nabla V_{\text{ext}}^{(\alpha)}(\mathbf{r}). \tag{38}$$

Here the correlation function of density fluctuations [2, 51, 71] has the common form $H_2^{(\alpha\alpha')}(\mathbf{r},\mathbf{r}') = \text{cov}(\hat{\rho}_\alpha(\mathbf{r}),\hat{\rho}_{\alpha'}(\mathbf{r}'))$, where the covariance of two operators $\hat{A}$ and $\hat{B}$ is defined in the standard way as $\text{cov}(\hat{A},\hat{B}) =$

$\langle\hat{A}\hat{B}\rangle - \langle\hat{A}\rangle\langle\hat{B}\rangle$. Equation (38) is analogous to the corresponding one-component identity of Ref. [26], which itself is recovered for the case of a single species, $M = \alpha = \alpha' = 1$.

A species-resolved version of Eq. (38), which involves also interparticle contributions, is given by

$$\beta\text{cov}(\hat{\mathbf{F}}_U^{\circ(\alpha)},\hat{\mathbf{F}}_U^{\circ(\alpha')}) = \Big\langle \sum_{i\in\mathcal{N}_\alpha}\sum_{j\in\mathcal{N}_{\alpha'}} \nabla_i\nabla_j u(\mathbf{r}^N)\Big\rangle$$
$$+ \delta_{\alpha\alpha'}\int d\mathbf{r}\rho_\alpha(\mathbf{r})\nabla\nabla V_{\text{ext}}^{(\alpha')}(\mathbf{r}), \tag{39}$$

where the species-resolved global force operator is

$$\hat{\mathbf{F}}_U^{\circ(\alpha)} = \int d\mathbf{r}\hat{\mathbf{F}}_U^{(\alpha)}(\mathbf{r}) = -\sum_{i\in\mathcal{N}_\alpha}\nabla_i\hat{U}. \tag{40}$$

Summing over both species labels α and α' in Eq. (39) and observing that $\sum_\alpha\sum_{i\in\mathcal{N}_\alpha}\nabla_i u(\mathbf{r}^N) = 0$ recovers Eq. (38).

Furthermore the density-force correlation sum rule [30] for the case of mixtures is

$$\langle\beta\hat{\mathbf{F}}_\alpha(\mathbf{r})\hat{\rho}_{\alpha'}(\mathbf{r}')\rangle = \delta_{\alpha\alpha'}\nabla'\rho_{2,\text{self}}^{(\alpha)}(\mathbf{r},\mathbf{r}'), \tag{41}$$

where the self two-body density distribution is defined as $\rho_{2,\text{self}}^{(\alpha)}(\mathbf{r},\mathbf{r}') = \langle\sum_{i\in\mathcal{N}_\alpha}\delta(\mathbf{r}-\mathbf{r}_i)\delta(\mathbf{r}'-\mathbf{r}_i)\rangle$ and the right hand side of Eq. (41) can alternatively be written as $\delta_{\alpha\alpha'}\rho(\mathbf{r})\nabla'\delta(\mathbf{r}-\mathbf{r}')$. The derivation of Eq. (41) can be based on the mixed second order invariance $0 = \delta^2\Omega/[\delta\boldsymbol{\epsilon}_\alpha(\mathbf{r})\delta V_{\text{ext}}^{(\alpha')}(\mathbf{r}')] = \delta\rho_{\alpha'}(\mathbf{r}')/\delta\boldsymbol{\epsilon}_\alpha(\mathbf{r}) = -\delta\mathbf{F}_\alpha(\mathbf{r})/\delta V_{\text{ext}}^{(\alpha')}(\mathbf{r}')$. Here the two alternative resulting expressions are obtained from exchanging the order of the two functional derivatives, re-writing via using that $\rho_{\alpha'}(\mathbf{r}') = \delta\Omega/\delta V_{\text{ext}}^{(\alpha')}(\mathbf{r}')$ and $\mathbf{F}_\alpha(\mathbf{r}) = -\delta\Omega/\delta\boldsymbol{\epsilon}_\alpha(\mathbf{r})$, and setting the species-resolved displacement fields to zero.

IV. HYPERFORCE SUM RULES FOR MIXTURES

A. Local hyperforce sum rules

We consider general observables $\hat{A}(\mathbf{r}^N,\mathbf{p}^N)$ and their corresponding equilibrium average $A = \langle\hat{A}(\mathbf{r}^N,\mathbf{p}^N)\rangle$. Following the argumentation of Ref. [31], the value of A is invariant under the species-resolved shifting transformation (8) and (9). Hence the functional derivative with respect to each shifting field vanishes,

$$\frac{\delta A[\{\boldsymbol{\epsilon}_{\alpha'}\}]}{\delta\boldsymbol{\epsilon}_\alpha(\mathbf{r})} = 0. \tag{42}$$

Using the explicit form of the equilibrium average as a phase space integral, one can re-write Eq. (42) in the
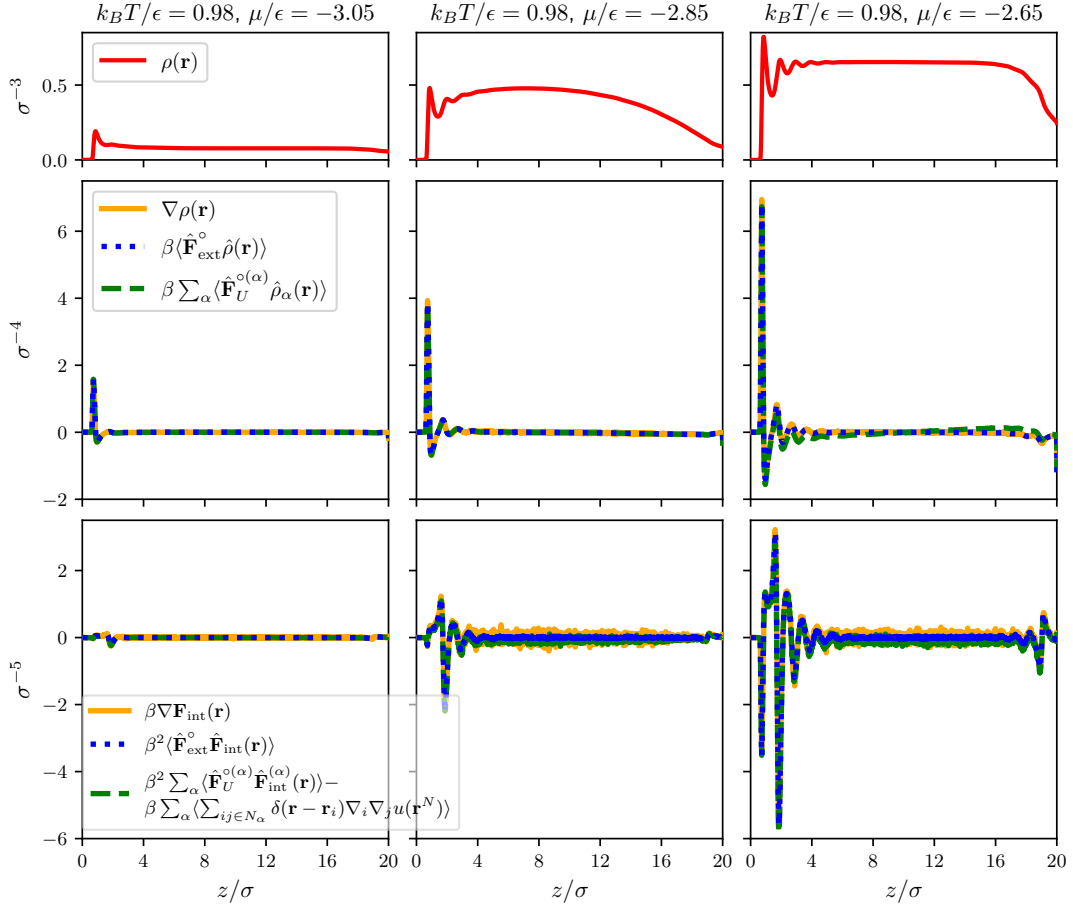
FIG. 2: Specific hyperforce correlation functions of the symmetrical Lennard-Jones mixture of Wilding *et al.* [55–61] at scaled temperature $k_B T/\epsilon = 0.98$ in the gas phase at chemical potential $\mu/\epsilon = -3.05$ (left column), in the mixed liquid phase at $\mu/\epsilon = -2.85$ (middle column), and in the demixed liquid phase at $\mu/\epsilon = -2.65$ (right column). The system is asymmetrically confined between an attractive wall (left) and a purely repulsive wall (right) and it is translationally invariant in the x and y directions. Top row: the total density profile $\rho(\mathbf{r}) = \rho_1(\mathbf{r}) + \rho_2(\mathbf{r})$ is shown as a function of the scaled distance z/σ across the pore. Middle row: the gradient of the density profile, $\nabla\rho(\mathbf{r}) = \partial\rho(z)/\partial z$, coincides numerically with the z-component of $\langle\beta\hat{\mathbf{F}}^\circ_{\text{ext}}\hat{\rho}(\mathbf{r})\rangle$, according to Eq. (57), and with the z-component of $\sum_\alpha\langle\beta\mathbf{F}_U^{\circ(\alpha)}\hat{\rho}_\alpha\rangle$, according to Eq. (58). Bottom row: the zz-component of the gradient of the agglomerated local interparticle force density, $\nabla\beta\mathbf{F}_{\text{int}}(\mathbf{r})$, coincides numerically with the zz-component of the correlation function $\langle\beta\hat{\mathbf{F}}^\circ_{\text{ext}}\hat{\mathbf{F}}_{\text{int}}(\mathbf{r})\rangle$, according to Eq. (60), and with the zz-component of $\sum_\alpha\langle\beta\hat{\mathbf{F}}_U^{\circ(\alpha)}\beta\hat{\mathbf{F}}_{\text{int}}^{(\alpha)}(\mathbf{r})\rangle - \sum_\alpha\langle\sum_{ij\in\mathcal{N}_\alpha}\delta(\mathbf{r}-\mathbf{r}_i)\nabla_i\nabla_j\beta u(\mathbf{r}^N)\rangle$, according to Eq. (61).

following more explicit form:

$$-\beta\left\langle\frac{\delta H[\{\boldsymbol{\epsilon}_{\alpha'}\}]}{\delta\boldsymbol{\epsilon}_\alpha(\mathbf{r})}\bigg|_{\{\boldsymbol{\epsilon}_{\alpha'}=0\}}\hat{A}\right\rangle + \left\langle\frac{\delta\hat{A}[\{\boldsymbol{\epsilon}_{\alpha'}\}]}{\delta\boldsymbol{\epsilon}_\alpha(\mathbf{r})}\bigg|_{\{\boldsymbol{\epsilon}_{\alpha'}=0\}}\right\rangle = 0,$$
(43)

where all partial shifting fields $\{\boldsymbol{\epsilon}_{\alpha'}(\mathbf{r})\}$ have been set to zero after the derivative is taken. Making the first term in Eq. (43) more explicit via its relationship to the partial force density operator (11) and also calculating the second term explicitly leads to the following species-resolved hyperforce sum rule:

$$\langle\beta\hat{\mathbf{F}}_\alpha(\mathbf{r})\hat{A}\rangle + \left\langle\sum_{i\in\mathcal{N}_\alpha}\delta(\mathbf{r}-\mathbf{r}_i)\nabla_i\hat{A}\right\rangle$$
$$+\nabla\cdot\left\langle\sum_{i\in\mathcal{N}_\alpha}\delta(\mathbf{r}-\mathbf{r}_i)\frac{\partial\hat{A}}{\partial\mathbf{p}_i}\mathbf{p}_i\right\rangle = 0,$$
(44)

where the observable $\hat{A}(\mathbf{r}^N,\mathbf{p}^N)$ can have general phase space dependence on $\mathbf{r}^N,\mathbf{p}^N$. Using the definition (20) of the species-resolved hyperforce observable $\hat{\mathbf{S}}_A^{(\alpha)}(\mathbf{r})$, we can put Eq. (44) into the more compact form

$$\mathbf{S}_A^{(\alpha)}(\mathbf{r}) + \langle\beta\hat{\mathbf{F}}_\alpha(\mathbf{r})\hat{A}\rangle = 0,$$
(45)

where the partial mean hyperforce density is $\mathbf{S}_A^{(\alpha)}(\mathbf{r}) = \langle \hat{\mathbf{S}}_A^{(\alpha)}(\mathbf{r})\rangle$.

For cases where $\hat{A}$ is independent of the degrees of freedom of species α, as denoted by $\hat{A}(\{\mathbf{r}_i,\mathbf{p}_i\}_{i\notin\mathcal{N}_\alpha})$ the right hand side of the species-resolved hyperforce density balance (44) vanishes, which leads to the remarkably simple result:

$$\langle \beta\hat{\mathbf{F}}_\alpha(\mathbf{r})\hat{A}(\{\mathbf{r}_i,\mathbf{p}_i\}_{i\notin\mathcal{N}_\alpha})\rangle = 0. \qquad (46)$$

Hence the total force density that acts on species α is uncorrelated with all observables that only depend on the degrees of freedom of the species that are different from α. As the average partial force density vanishes in equilibrium, $\mathbf{F}_\alpha(\mathbf{r}) = 0$ according to Eq. (12), the relationship (46) implies trivially that also $\mathrm{cov}(\hat{\mathbf{F}}_\alpha(\mathbf{r}), \hat{A}(\{\mathbf{r}_i,\mathbf{p}_i\}_{i\notin\mathcal{N}_\alpha})) = 0$.

In case that the considered observable is independent of momenta and hence is a function of only the positions, i.e., $\hat{A}(\mathbf{r}^N)$, the last, momentum-dependent term on the left hand side of Eq. (44) vanishes, and we obtain

$$\langle \beta\hat{\mathbf{F}}_\alpha(\mathbf{r})\hat{A}(\mathbf{r}^N)\rangle + \Big\langle \sum_{i\in\mathcal{N}_\alpha}\delta(\mathbf{r}-\mathbf{r}_i)\nabla_i\hat{A}(\mathbf{r}^N)\Big\rangle = 0. \quad (47)$$

Using the standard splitting (7) of the position-dependent total force operator into interparticle, external, and kinetic contributions allows one to re-write Eq. (47) in the following more explicit form:

$$\langle \beta\hat{\mathbf{F}}_{\mathrm{int}}^{(\alpha)}(\mathbf{r})\hat{A}(\mathbf{r}^N)\rangle - \langle \hat{\rho}_\alpha(\mathbf{r})\hat{A}(\mathbf{r}^N)\rangle\nabla\beta V_{\mathrm{ext}}^{(\alpha)}(\mathbf{r})$$
$$-\nabla\langle \hat{\rho}_\alpha(\mathbf{r})\hat{A}(\mathbf{r}^N)\rangle + \Big\langle \sum_{i\in\mathcal{N}_\alpha}\delta(\mathbf{r}-\mathbf{r}_i)\nabla_i\hat{A}(\mathbf{r}^N)\Big\rangle = 0.$$
$$(48)$$

For cases where the observable of interest depends only on the position variables of an individual species α', as denoted by $\hat{A}(\{\mathbf{r}_i\}_{i\in\mathcal{N}_{\alpha'}})$, we can particularize Eq. (47) further:

$$\langle \beta\hat{\mathbf{F}}_\alpha(\mathbf{r})\hat{A}(\{\mathbf{r}_i\}_{i\in\mathcal{N}_{\alpha'}})\rangle$$
$$+ \delta_{\alpha\alpha'}\Big\langle \sum_{i\in\mathcal{N}_\alpha}\delta(\mathbf{r}-\mathbf{r}_i)\nabla_i\hat{A}(\{\mathbf{r}_i\}_{i\in\mathcal{N}_{\alpha'}})\Big\rangle = 0, \quad (49)$$

such that the second term is only nonvanishing in the intraspecies case, $\alpha = \alpha'$.

B. Global hyperforce sum rules

Integrating Eq. (48) over position $\mathbf{r}$ and exploiting that the diffusive terms vanish in systems enclosed by walls allows one to obtain the following global hyperforce sum rule:

$$\langle \beta\hat{\mathbf{F}}_{\mathrm{ext}}^{\circ(\alpha)}\hat{A}\rangle + \langle \beta\hat{\mathbf{F}}_{\mathrm{int}}^{\circ(\alpha)}\hat{A}\rangle + \Big\langle \sum_{i\in\mathcal{N}_\alpha}\nabla_i\hat{A}\Big\rangle = 0. \quad (50)$$

Here the global external force operator for species α is defined as the sum over all external forces that act on this species, i.e., $\hat{\mathbf{F}}_{\mathrm{ext}}^{\circ(\alpha)} = -\sum_{i\in\mathcal{N}_\alpha}\nabla_i V_{\mathrm{ext}}^{(\alpha)}(\mathbf{r}_i)$ and correspondingly for the species-resolved global interparticle force $\hat{\mathbf{F}}_{\mathrm{int}}^{\circ(\alpha)} = -\sum_{i\in\mathcal{N}_\alpha}\nabla_i u(\mathbf{r}^N)$. Building the sum of both contributions allows one to relate to the species-resolved global potential force operator (40) as $\hat{\mathbf{F}}_U^{\circ(\alpha)} = \hat{\mathbf{F}}_{\mathrm{int}}^{\circ(\alpha)} + \hat{\mathbf{F}}_{\mathrm{ext}}^{\circ(\alpha)}$. This allows one to rewrite Eq. (50) in a more compact form,

$$\langle \beta\hat{\mathbf{F}}_U^{\circ(\alpha)}\hat{A}\rangle + \Big\langle \sum_{i\in\mathcal{N}_\alpha}\nabla_i\hat{A}\Big\rangle = 0. \quad (51)$$

Note that the partial interparticle forces need not vanish individually, yet when summed over all species $\sum_\alpha\hat{\mathbf{F}}_{\mathrm{int}}^{\circ(\alpha)} = 0$, as follows from Newton's third law or, analogously, from the global translational invariance of the interparticle potential $u(\mathbf{r}^N)$ [24].

Summing the identity (50) over all species yields

$$\langle \beta\hat{\mathbf{F}}_{\mathrm{ext}}^\circ\hat{A}\rangle + \Big\langle \sum_i\nabla_i\hat{A}\Big\rangle = 0, \quad (52)$$

where we have defined the global external force as $\hat{\mathbf{F}}_{\mathrm{ext}}^\circ = \sum_\alpha\hat{\mathbf{F}}_{\mathrm{ext}}^{\circ(\alpha)}$ and have exploited that the global interparticle force operator vanishes, $\sum_\alpha\hat{\mathbf{F}}_{\mathrm{int}}^{\circ(\alpha)} = 0$, as described above. We have simplified the summation over particles in Eq. (52) according to $\sum_i = \sum_\alpha\sum_{i\in\mathcal{N}_\alpha}$, where the sum on the left hand side runs over all particles in the system. The form of the sum rule (51) is identical to the corresponding result for one-component systems [31].

C. Local sum rules for specific observables

We apply the general hyperforce framework described in Sec. IV B above to several exemplary choices for the 'hyperobservable' $\hat{A}$, following the outline of the single-component treatment in Ref. [31]. As an initial consistency check, the trivial choice $\hat{A} = 1$ leads via Eq. (49) [or alternatively via the simple Eq. (46)] directly to the partial force balance relationship (10). Choosing the partial density operator $\hat{A} = \hat{\rho}_{\alpha'}(\mathbf{r}') = \sum_{i\in\mathcal{N}_{\alpha'}}\delta(\mathbf{r}'-\mathbf{r}_i)$ and applying Eq. (49) yields

$$\langle \beta\hat{\mathbf{F}}_\alpha(\mathbf{r})\hat{\rho}_{\alpha'}(\mathbf{r}')\rangle = \delta_{\alpha\alpha'}\nabla'\rho_{2,\mathrm{self}}^{(\alpha)}(\mathbf{r},\mathbf{r}'), \quad (53)$$

which is the density-force correlation sum rule (41). Taking the interparticle potential energy $\hat{A} = u(\mathbf{r}^N)$ leads via Eq. (47) to

$$\langle \beta\hat{\mathbf{F}}_\alpha(\mathbf{r})u(\mathbf{r}^N)\rangle = \mathbf{F}_{\mathrm{int}}^{(\alpha)}(\mathbf{r}). \quad (54)$$

Furthermore the (scaled) center of mass of all particles of species α, given by $\hat{A} = \sum_{i\in\mathcal{N}_{\alpha'}}\mathbf{r}_i$, leads via Eq. (49) to the following identity:

$$-\Big\langle \beta\hat{\mathbf{F}}_\alpha(\mathbf{r})\sum_{i\in\mathcal{N}_{\alpha'}}\mathbf{r}_i\Big\rangle = \delta_{\alpha\alpha'}\mathbb{1}\rho_\alpha(\mathbf{r}), \quad (55)$$

where we recall $\mathbb{1}$ as the $d \times d$-unit matrix with d indicating the spatial dimensionality.

D. Global sum rules for specific observables

We formulate several global sum rules that arise from making specific choices of hyperobservables. Our aim below in Sec. V will be to demonstrate in simulations the validity of these sum rules and to show the accessibility of the correlation functions that are involved.

We first address the partial density operator. In the general sum rule (51) we set $\hat{A} = \hat{\rho}_{\alpha'}(\mathbf{r})$ and use the simplification $\langle \sum_{i \in \mathcal{N}_\alpha} \nabla_i \hat{\rho}_{\alpha'}(\mathbf{r}) \rangle = -\delta_{\alpha\alpha'} \nabla \rho_\alpha(\mathbf{r})$, where we recall that no summation over doubles species indices is implied in our notation. Then one obtains the following sum rule:

$$\langle \beta \hat{\mathbf{F}}_U^{\circ(\alpha)} \hat{\rho}_{\alpha'}(\mathbf{r}) \rangle - \delta_{\alpha\alpha'} \nabla \rho_\alpha(\mathbf{r}) = 0, \qquad (56)$$

which applies to all combinations of α, α'. Summing Eq. (56) over all pairs of species yields

$$\langle \beta \hat{\mathbf{F}}_{\text{ext}}^{\circ} \hat{\rho}(\mathbf{r}) \rangle - \nabla \rho(\mathbf{r}) = 0, \qquad (57)$$

which is analogous in form to the one-component hyperforce sum rule for the density operator [31]. The agglomerated density operator is obtained by summing over all species according to $\hat{\rho}(\mathbf{r}) = \sum_\alpha \hat{\rho}_\alpha(\mathbf{r})$ and we recall $\hat{\mathbf{F}}_{\text{ext}}^{\circ}$ as the agglomerated external force.

Specializing Eq. (56) to the case $\alpha = \alpha'$ and summing over the remaining species index gives the following alternative form:

$$\left\langle \sum_\alpha \beta \hat{\mathbf{F}}_U^{\circ(\alpha)} \hat{\rho}_\alpha(\mathbf{r}) \right\rangle - \nabla \rho(\mathbf{r}) = 0, \qquad (58)$$

where the first (correlation) term differs from that in Eq. (57): i) interparticle interactions contribute and ii) only intraspecies correlations between forces and densities occur. Equations (57) and (58) are both suitable for situations where one is interested in the behaviour of the agglomerated density profile $\rho(\mathbf{r})$ rather than its partial variants $\rho_\alpha(\mathbf{r})$, as can be advantageous in situations of demixing phase separation.

We next consider the species-resolved interparticle force density operator $\hat{A} = \beta \hat{\mathbf{F}}_{\text{int}}^{(\alpha')}(\mathbf{r})$, of which we recall the explicit form $\beta \hat{\mathbf{F}}_{\text{int}}^{(\alpha')}(\mathbf{r}) = -\sum_{i \in \mathcal{N}_{\alpha'}} \delta(\mathbf{r} - \mathbf{r}_i) \nabla_i \beta u(\mathbf{r}^N)$. Then specializing the global sum rule (51) yields

$$\langle \beta \hat{\mathbf{F}}_U^{\circ(\alpha)} \beta \hat{\mathbf{F}}_{\text{int}}^{(\alpha')}(\mathbf{r}) \rangle + \left\langle \sum_{i \in \mathcal{N}_\alpha} \nabla_i \beta \hat{\mathbf{F}}_{\text{int}}^{(\alpha')}(\mathbf{r}) \right\rangle = 0. \qquad (59)$$

Note that $\hat{\mathbf{F}}_{\text{int}}^{(\alpha')}(\mathbf{r})$ will in general depend also on further species $\alpha' \neq \alpha$, such that the gradient in the second term in Eq. (59) will in general be nonzero; this situation is different from the mechanism in Eq. (49) where

$\hat{A}(\{\mathbf{r}_i\}_{i \in \mathcal{N}_{\alpha'}})$ depends *solely* on the positions of species α'.

Furthermore we address the thermally scaled agglomerated interparticle force density $\hat{A} = \beta \hat{\mathbf{F}}_{\text{int}}(\mathbf{r}) = \sum_\alpha \hat{\beta} \mathbf{F}_{\text{int}}^{(\alpha)}(\mathbf{r})$. Then from Eq. (52) and Newton's third law one obtains the following global sum rule:

$$\langle \beta \hat{\mathbf{F}}_{\text{ext}}^{\circ} \beta \hat{\mathbf{F}}_{\text{int}}(\mathbf{r}) \rangle - \nabla \beta \mathbf{F}_{\text{int}}(\mathbf{r}) = 0. \qquad (60)$$

One obtains an alternative to Eq. (60) by first specializing Eq. (59) to the case of equal species, $\alpha = \alpha'$, and then building the sum over the remaining joint species index. Simplifying the result yields:

$$\sum_\alpha \langle \beta \hat{\mathbf{F}}_U^{\circ(\alpha)} \beta \hat{\mathbf{F}}_{\text{int}}^{(\alpha)}(\mathbf{r}) \rangle$$
$$- \sum_\alpha \left\langle \sum_{ij \in \mathcal{N}_\alpha} \delta(\mathbf{r} - \mathbf{r}_i) \nabla_i \nabla_j \beta u(\mathbf{r}^N) \right\rangle - \nabla \beta \mathbf{F}_{\text{int}}(\mathbf{r}) = 0. \qquad (61)$$

Hence both sum rules (60) and (61) feature the thermally-scaled negative gradient of the agglomerated interparticle force density $-\nabla \beta \mathbf{F}_{\text{int}}(\mathbf{r})$ as the last term on the left hand sides.

We test the sum rules (57), (58), (60), and (61) in simulations, as described in the following.

V. SIMULATION RESULTS

To illustrate the gauge correlation theory we apply it to a concrete system and hence consider the prototypical binary Lennard-Jones mixture in three spatial dimensions. The system is characterized by pair potentials $\phi_{\alpha\alpha'}(r)$ that act between particles of species α and α'. The species-labelled Lennard-Jones potential is thereby given by

$$\phi_{\alpha\alpha'}(r) = 4\epsilon_{\alpha\alpha'} \left[\left(\frac{\sigma_{\alpha\alpha'}}{r} \right)^{12} - \left(\frac{\sigma_{\alpha\alpha'}}{r} \right)^6 \right], \qquad (62)$$

where r is the separation distance between the two particles, $\epsilon_{\alpha\alpha'}$ are energy parameters, and $\sigma_{\alpha\alpha'}$ are length-scales, with the species indices taking on values $\alpha, \alpha' = 1, 2$ in a two-component system and implying the symmetry $\phi_{12}(r) = \phi_{21}(r)$.

A. Bulk force-force correlation structure

We first address the pair gauge correlation structure of a bulk liquid using the Lennard-Jones parameterization due to Kob and Andersen [62, 63]. The fundamental length scale σ and energy scale ϵ are taken to be those of the first component $\alpha = 1$, such that $\sigma_{11} = \sigma$ and $\epsilon_{11} = \epsilon$. The intraspecies interactions amongst particles of species $\alpha = 2$ are characterized by a smaller length scale, $\sigma_{22} = 0.88\sigma$, and weakened energy scale, $\epsilon_{22} = 0.5\epsilon$. The cross species length scale is reduced, $\sigma_{12} =$

0.8σ, and the cross interactions are strengthened, $\epsilon_{12} = 1.5\epsilon$, as compared to both intraspecies pair potentials.

We use adaptive Brownian dynamics [72] to sample the gauge correlation functions of the bulk liquid at thermal equilibrium in the canonical ensemble. We use a cubic simulation box with lateral size 10σ and total particle number $N = 844$. Hence the total bulk density is $\rho_b = N/V = 0.844\sigma^{-3}$ and the partial bulk densities are $\rho_1^b\sigma^3 = 0.591$ and $\rho_2^b\sigma^3 = 0.253$, and we choose the temperature as $k_BT/\epsilon = 1.1$. We truncate all pair potentials at a cutoff distance $r_c = 2.5\sigma$ and potential shifts are applied such that each $\phi_{\alpha\alpha'}(r)$ is continuous at r_c. We have used an initial simulation period of temporal length $5\tau_B$ for equilibration, with Brownian time scale $\tau_B = \sigma^2 D_0 k_B T/\epsilon$, where D_0 is the single-particle diffusion constant. The data is collected over 25 runs, which amounts to an overall time $4000\tau_B$ that consists of $\sim 6.5 \cdot 10^7$ adaptive time steps [72]. The parameters for the adaptive Brownian dynamics tolerance criterium are set as 0.1 (relative tolerance) and 0.01 (absolute tolerance); see Ref. [72] for details.

In Fig. 1 we display results for the partial pair distribution functions, for the force-gradient correlation functions, and for the force-force correlation functions. The partial pair distribution functions $g_{\alpha\alpha'}(r)$ display pronounced spatial structuring that is typical of the liquid state, see the first row in Fig. 1. Both $g_{11}(r)$ and $g_{12}(r)$ possess pronounced first peaks, which are indicative of the formation of nearest neighbour coordination shells. The subsequent decay for increasing distance r/σ is damped oscillatory, on the linear scale considered here. The first peak of $g_{22}(r)$ is less strongly pronounced than for the 11- and 12-pairs, but the decay towards larger values of r/σ is also damped oscillatory, as is expected from the general theory of asymptotic decay of correlations in liquids [3, 73–76], which ascertains common type of decay for all partial pair distribution functions. The agglomerated pair distribution function $g(r)$ displays rich oscillatory structure. This structuring arises from the linear combination of the underlying partial contributions, see the fourth panel in the first row of Fig. 1.

Results for the force-gradient correlation function $g_{\nabla f}^{(\alpha\alpha')}(r)$ are shown in the second and third row of Fig. 1, where we display, respectively, the parallel and the perpendicular tensor components. Simulation results are obtained by sampling the force gradients via finite differences, which are built by performing virtual particle displacements [29]. This 'direct' method is of universal applicability to general many-body interparticle interactions, such as the monatomic water model [77] and the three-body gel former [78–80], both of which are special parameter choices of the general Stillinger-Weber model [81]. The finite difference method also circumvents the need to implement Hessians of interparticle potentials explicitly

For the present pairwise-interacting mixture, each partial force-gradient pair correlation function is related to the corresponding partial pair distribution function $g_{\alpha\alpha'}(r)$ and the Hessian of the pair potential $\nabla\nabla\phi_{\alpha\alpha'}(r)$, see Eq. (32) and the dotted lines in the second and third row of Fig. 1. The identity (32) is verified numerically, see Fig. 1. The parallel and perpendicular tensor components display respectively a strong positive and negative first peak, as can be expected from the underlying second and first derivatives of the respective pair potential with respect to distance. Both tensor components strictly vanish beyond the potential truncation distance r_c. The perpendicular component displays a positive overshoot for each pair of species. We attribute the effect to the presence of interparticle attraction, see Ref. [80] for a comparison of results for the one-component Lennard-Jones fluid and for the purely repulsive (also one-component) Weeks-Chandler-Andersen fluid, where in the latter model the effect is absent.

Results for the partial force-force pair correlation functions $g_{ff}^{(\alpha\alpha')}(r)$ are shown in the fourth and fifth row of Fig. 1. We recall that this correlation function measures the correlation of the sum of all interparticle forces acting on each particle of the considered pair. No simplification arises that would be similar to that for the above force gradient correlation function $g_{\nabla f}^{(\alpha\alpha')}(r)$. Performing the sampling of the force-force gradient correlation function is straightforward, in particular when using methods that already provide direct access to forces, as is the case for the present adaptive Brownian dynamics or, similarly, in Molecular Dynamics. A description of a suitable choice of coordinate system that facilitates straightforward access to the parallel and perpendicular tensor components is given in Ref. [29].

The partial force-force correlation functions again display rich spatial structuring. The parallel component has a strong first negative peak, as is indicative of anti-correlated forces on two mutually interacting particles. Note that the negative sign is indicative of anticorrelation both for repulsion in the core region and for the longer-ranged attraction. The perpendicular tensor component has smaller amplitude and smoother variation with distance. The two tensor components, see Eqs. (33) and (34), of the species-resolved 3g-sum rule (29), as well as the species-agglomerated sum rules, see Eqs. (36) and (37), are satisfied to excellent accuracy. We hence conclude that the gauge correlation framework offers significant and physically meaningful insight into the spatial structure of bulk liquid mixtures.

B. Confinement between parallel walls

To consider a second model fluid, we follow Wilding *et al.* [55–61], who investigated a symmetrical Lennard-Jones mixture with a single common lengthscale $\sigma_{11} = \sigma_{22} = \sigma_{12} = \sigma$. The two intraspecies interaction strengths are identical, $\epsilon_{11} = \epsilon_{22} = \epsilon$, and the cross-species interaction strength is weakened by comparison, $\epsilon_{12} = 0.7\epsilon$. The cutoff radius is again chosen as $r_c = 2.5\sigma$ and no potential shift is applied. We use grand canonical

Monte Carlo simulations [82–84] to generate equilibrium data. The system exhibits intricate phase behaviour, including gas-liquid and liquid-liquid phase coexistence phenomena, which were recently re-addressed using neural density functional learning [50].

We demonstrate the applicability of the hyperforce framework to spatially inhomogeneous systems by considering confinement in a planar asymmetric slit pore. The left wall is thereby taken to be of Lennard-Jones 9–3 type [57]: $V_{\text{ext},L}(z) = \epsilon[(2/15)(\sigma/z)^9 - (\sigma/z)^3]$, where z measures the distance from the wall and we recall ϵ as the common energy scale. The right wall is purely repulsive: $V_{\text{ext},R}(z) = 4\epsilon_w[(\sigma/z)^{12} - (\sigma/z)^6 + 1/4]$, where the wall potential strength is taken to be $\epsilon_w = 10\epsilon$, and the cutoff is at $z_c = 2^{1/6}\sigma$. The total external potential is then given by the combination $V_{\text{ext}}(z) = V_{\text{ext},L}(z) + V_{\text{ext},R}(L_z - z)$, with simulation box size L_z in the z-direction. We choose $L_z = 20\sigma + 2^{1/6}\sigma = 21.122\sigma$ and take the box size in the two lateral directions to be 5σ. For each of the three statepoints considered we have carried out $2 \cdot 10^9$ (gas) and $3 \cdot 10^9$ (mixed and demixed liquid) grand canonical Monte Carlo single particle moves. Each move consists of either a position displacement with maximal length 0.2σ or particle insertion/deletion attempt, performed with probability 0.1. We collect data after an equilibration period of $3 \cdot 10^5$ Monte Carlo steps.

Fig. 2 shows our simulation results for the specific hyperforce correlation functions laid out in Sec. IV D. These correlation functions are chosen specifically to facilitate access both to the gradient of the density profile and to the gradient of the localized interparticle force density. We hence consider the sum rules (57) and (58) for the gradient of the total density profile, and the identities (60) and (61) for the gradient of the agglomerated interparticle force density. We choose three statepoints, as typical for the gas, the mixed liquid, and the demixed liquid phase. The comparisons shown in Fig. 2 demonstrate that in all cases considered, we find the sum rules to be satisfied.

VI. CONCLUSIONS

In summary, we have explored the consequences of gauge invariance with respect to species-resolved phase space shifting in multi-component classical many-body systems. The gauge transformation constitutes a species-specific canonical transformation that acts on the fundamental position and momentum degrees of freedom. The transformation is represented by differential operators that act on general phase space observables and that feature Lie algebra commutator structure. The geometric nature of the gauge transformation, see Ref. [33] for an in-depth description, renders the framework generally applicable to arbitrary phase space functions $\hat{A}$ as the 'hyperobservable' of interest. The hyperobservable can be a bespoke order parameter that is relevant for

the physics of the system under consideration or, alternatively, it can be chosen as a more standard observable, such as the partial one-body density and force density observables, as we have considered here in our simulation work.

We have described the rich formal gauge correlation structure that emerges in mixtures, where the hyperobservable, in analogy to the Hamiltonian itself [43], generates corresponding spatially-resolved hyperforce density observables via phase space differentiation. Upon building the thermal equilibrium average, the mean partial one-body hyperforce density is related, in a formally exact way, via equilibrium sum rules to the correlation of the hyperobservable with the spatially localized force density. We have described in detail several relevant special cases of these sum rules that are relevant for mixtures, such as, e.g., arising from the absence of the dependence on specific species, which leads to formal simplification.

Turning to the two-body level of the gauge correlation functions, we have generalized the emerging two-body force-force and force-gradient correlation framework, as were formulated originally for pure systems [29, 30], to multi-component systems. Our corresponding simulation work for the Kob-Andersen model, in its liquid phase, has shown that deep insights into the liquid structure can be gained specifically from the partial force-force and force-gradient correlation functions. We found all corresponding sum rules to be satisfied numerically. We recall that their validity hinges on thermal equilibrium. Hence our present investigation could serve as a platform to shed new light on the rich topic of the nonequilibrium nature of glasses that arise from performing a temperature quench of the liquid. We refer to Ref. [34] for the formulation of dynamical hypercurrent sum rules that arise from the dynamical generalization of phase space shifting.

We have demonstrated the applicability of the gauge correlation framework to spatially inhomogeneous systems by carrying out simulations for a symmetrical Lennard-Jones system previously investigated by Wilding et al. [55–61] in the context of bulk phase behaviour and associated interfacial physics. We have ascertained that both the gradient of the density profile and the gradient of the one-body force density distribution are accessible via corresponding hyperforce correlation functions, see Fig. 2 and the description given in Sec. V B.

The fact that the hyperobservable can be of very general nature allows one to address concrete applications in flexible ways. For further specific examples, we refer to Refs. [42, 43] for investigations of the hyperfluctuation profile that is associated with a clustering order parameter and to Refs. [85–87] for the local thermal susceptibility, which arises from addressing the entropy. Choosing the species-resolved number of particles, $\hat{A} = N_\alpha$, leads to partial versions of the local compressibility [87–91]. In future work, it would be interesting to investigate connections to the reduced-variance (force-sampling) [92–95] and mapped averaging [96–98] schemes. In particular the

two-body framework of Sec. III B offers potential for such use; note that Eqs. (33) and (34) can be viewed as differential equations for the partial pair distribution functions, provided that (simulation) results for the partial force-force correlation functions are available.

The present theory can form a supporting role for neural functional construction [39–50] and the sum rules have significant potential for serving as diagnostic tools to assess the self-consistency of numerical predictions. The hyperforce gauge correlation identities tie in particularly with the hyperdensity functional framework for the behaviour of general observables in spatially inhomogeneous systems [42, 43], as follows from the fundamental Mermin-Evans density functional map [51, 99].

Data availability

Simulation data will be openly available at Zenodo [100].

Acknowledgments

[1] R. Evans, D. Frenkel, and M. Dijkstra, From simple liquids to colloids and soft matter, Phys. Today **72**, 38 (2019).

[2] J. P. Hansen and I. R. McDonald, *Theory of Simple Liquids*, 4th ed. (Academic Press, London, 2013).

[3] P. Cats, R. Evans, A. Härtel, and R. van Roij, Primitive model electrolytes in the near and far field: Decay lengths from DFT and simulations, J. Chem. Phys. **154**, 124504 (2021).

[4] T. H. N. Minh, B. Rotenberg, and S. Marbach, Ionic fluctuations in finite volumes: fractional noise and hyperuniformity, Faraday Discuss. **246**, 225 (2023).

[5] T. H. N. Minh, J. Kim, G. Pireddu, I. Chubak, S. Nair, and B. Rotenberg, Electrical noise in electrolytes: a theoretical perspective, Faraday Discuss. **246**, 198 (2023).

[6] S. J. Cox, Dielectric response with short-ranged electrostatics, Proc. Natl. Acad. Sci. **117**, 19746 (2020).

[7] A. T. Bui and S. J. Cox, A classical density functional theory for solvation across length scales, J. Chem. Phys. **161**, 104103 (2024).

[8] A. T. Bui and S. J. Cox, Learning classical density functionals for ionic fluids, Phys. Rev. Lett. **134**, 148001 (2025).

[9] A. T. Bui and S. J. Cox, A first principles approach to electromechanics in liquids, J. Phys.: Condens. Matter **37**, 285101 (2025).

[10] A. T. Bui and S. J. Cox, Dielectrocapillarity for exquisite control of fluids, arXiv:2503.09855.

[11] E. D. Cubuk, S. S. Schoenholz, J. M. Rieser, B. D. Malone, J. Rottler, D. J. Durian, E. Kaxiras, and A. J. Liu, Identifying structural flow defects in disordered solids using machine-learning methods, Phys. Rev. Lett. **114**, 108001 (2015).

[12] G. M. Hocky, T. E. Markland, and D. R. Reichman, Growing point-to-set length scale correlates with growing relaxation times in model supercooled liquids, Phys. Rev. Lett. **108**, 225506 (2012).

[13] A. Malins, J. Eggers, H. Tanaka, and C. P. Royall, Lifetimes and lengthscales of structural motifs in a model glassformer, Faraday Discuss. **167**, 405 (2013).

[14] F. Turci, C. P. Royall, and T. Speck, Nonequilibrium phase transition in an atomistic glassformer: the connection to thermodynamics, Phys. Rev. X **7**, 031028 (2017).

[15] E. Noether, Invariante Variationsprobleme, Nachr. d. König. Gesellsch. d. Wiss. zu Göttingen, Math.-Phys. Klasse, **235**, 183 (1918). English translation by M. A. Tavel: Invariant variation problems. Transp. Theo. Stat. Phys. **1**, 186 (1971); for a version in modern typesetting see: Frank Y. Wang, arXiv:physics/0503066v3 (2018).

[16] N. Byers, E. Noether's discovery of the deep connection between symmetries and conservation laws, arXiv:physics/9807044 (1998).

[17] J. C. Baez and B. Fong, A Noether theorem for Markov processes, J. Math. Phys. **54**, 013301 (2013).

[18] I. Marvian and R. W. Spekkens, Extending Noether's theorem by quantifying the asymmetry of quantum states, Nat. Commun. **5**, 3821 (2014).

[19] S. Sasa and Y. Yokokura, Thermodynamic entropy as a Noether invariant, Phys. Rev. Lett. **116**, 140601 (2016).

[20] S. Sasa, S. Sugiura, and Y. Yokokura, Thermodynamical path integral and emergent symmetry, Phys. Rev. E **99**, 022109 (2019).

[21] M. Revzen, Functional integrals in statistical physics, Am. J. Phys. **38**, 611 (1970).

[22] J. C. Baez, Getting to the bottom of Noether's theorem, arXiv:2006.14741.

[23] A. Bravetti, M. A. Garcia-Ariza, and D. Tapias, Thermodynamic entropy as a Noether invariant from contact geometry, Entropy **25**, 1082 (2023).

[24] S. Hermann and M. Schmidt, Noether's theorem in statistical mechanics, Commun. Phys. **4**, 176 (2021).

[25] S. Hermann and M. Schmidt, Why Noether's theorem applies to statistical mechanics, J. Phys.: Condens. Matter **34**, 213001 (2022); (Topical Review).

[26] S. Hermann and M. Schmidt, Variance of fluctuations from Noether invariance, Commun. Phys. **5**, 276 (2022).

[27] S. Hermann and M. Schmidt, Force balance in thermal quantum many-body systems from Noether's theorem, J. Phys. A: Math. Theor. **55**, 464003 (2022). *(Special Issue: Claritons and the Asymptotics of ideas: the Physics of Michael Berry).*

[28] S. M. Tschopp, F. Sammüller, S. Hermann, M. Schmidt, and J. M. Brader, Force density functional theory in- and out-of-equilibrium, Phys. Rev. E **106**, 014115 (2022).

[29] F. Sammüller, S. Hermann, D. de las Heras, and M. Schmidt, Noether-constrained correlations in equilibrium liquids, Phys. Rev. Lett. **130**, 268203 (2023).

[30] S. Hermann, F. Sammüller, and M. Schmidt, Noether invariance theory for the equilibrium force structure of soft matter, J. Phys. A: Math. Theor. **57**, 175001 (2024).

[31] S. Robitschko, F. Sammüller, M. Schmidt, and S. Hermann, Hyperforce balance from thermal Noether invariance of any observable, Commun. Phys. **7**, 103 (2024).

[32] J. Müller, S. Hermann, F. Sammüller, and M. Schmidt, Gauge invariance of equilibrium statistical mechanics, Phys. Rev. Lett. **133**, 217101 (2024); Editors' Suggestion; PRL's Collection of the Year 2024; Featured in Physics **17**, 163 (2024) by B. Rotenberg.

[33] J. Müller, F. Sammüller, and M. Schmidt, Why gauge invariance applies to statistical mechanics, J. Phys. A: Math. Theor. **58**, 125003 (2025).

[34] J. Müller, F. Sammüller, and M. Schmidt, Dynamical gauge invariance of statistical mechanics, arXiv:2504.17599.

[35] B. Rotenberg, Viewpoint: Symmetry spotted in statistical mechanics, Physics **17**, 163 (2024).

[36] J. L. Miller, Gauge invariance applies to statistical mechanics too, Physics Today **78**, 11 (2025); Cover image of the February 2025 issue **78** (2).

[37] R. Zwanzig, *Nonequilibrium Statistical Mechanics* (Oxford University Press, Oxford, 2001).

[38] M. Krüger and M. Fuchs, Non-equilibrium relation between mobility and diffusivity of interacting Brownian particles under shear, Prog. Theo. Phys. Suppl. **184**, 172 (2010).

[39] D. de las Heras, T. Zimmermann, F. Sammüller, S. Hermann, and M. Schmidt, Perspective: How to overcome dynamical density functional theory, J. Phys.: Condens. Matter **35**, 271501 (2023); (Invited Perspective).

[40] F. Sammüller, S. Hermann, D. de las Heras, and M. Schmidt, Neural functional theory for inhomogeneous fluids: Fundamentals and applications, Proc. Natl. Acad. Sci. **120**, e2312484120 (2023).

[41] F. Sammüller, S. Hermann, and M. Schmidt, Why neural functionals suit statistical mechanics, J. Phys.: Condens. Matter **36**, 243002 (2024); (Topical Review).

[42] F. Sammüller, S. Robitschko, S. Hermann, and M. Schmidt, Hyperdensity functional theory of soft matter, Phys. Rev. Lett. **133**, 098201 (2024); Editors' Suggestion.

[43] F. Sammüller and M. Schmidt, Why hyperdensity functionals describe any equilibrium observable, J. Phys.: Condens. Matter **37**, 083001 (2025); (Topical Review).

[44] F. Sammüller and M. Schmidt, Neural density functionals: Local learning and pair-correlation matching, Phys. Rev. E **110**, L032601 (2024); (Letter, Editors' Suggestion).

[45] T. Zimmermann, F. Sammüller, S. Hermann, M. Schmidt, and D. de las Heras, Neural force functional for non-equilibrium many-body colloidal systems, Mach. Learn.: Sci. Technol. **5**, 035062 (2024).

[46] F. Sammüller, M. Schmidt, and R. Evans, Neural density functional theory of liquid-gas phase coexistence, Phys. Rev. X **15**, 011013 (2025); Featured in Physics **18**, 17 (2025).

[47] M. Buchanan, Machine learning predicts liquid-gas transition, Physics **18**, 17 (2025).

[48] S. M. Kampa, F. Sammüller, M. Schmidt, and R. Evans, Metadensity functional theory for classical fluids: Extracting the pair potential, Phys. Rev. Lett. **134**, 107301 (2025); PRL Editors' Suggestion.

[49] F. Sammüller and M. Schmidt, Determining the chemical potential via universal density functional learning arXiv:2506.15608.

[50] S. Robitschko, F. Sammüller, M. Schmidt, and R. Evans, Learning the bulk and interfacial physics of liquid-liquid phase separation with neural density functionals, J. Chem. Phys. (Communication, submitted).

[51] R. Evans, The nature of the liquid-vapour interface and other topics in the statistical mechanics of non-uniform, classical fluids, Adv. Phys. **28**, 143 (1979).

[52] M. M. Telo da Gama and R. Evans, The structure and surface tension of the liquid-vapour interface near the upper critical end point of a binary mixture of Lennard-Jones fluids: I. The two phase region, Mol. Phys. **48**, 229 (1983).

[53] M. M. Telo da Gama and R. Evans, The structure and surface tension of the liquid-vapour interface near the upper critical end point of a binary mixture of Lennard-Jones fluids: II. The three phase region and the Cahn wetting transition, Mol. Phys. **48**, 251 (1983).

[54] I. Napari, A. Laaksonen, V. Talanquer, and D. W. Oxtoby, A density functional study of liquid-liquid interfaces in partially miscible systems, J. Chem. Phys. **110**, 5906 (1999).

[55] N. B. Wilding, Critical end point behavior in a binary fluid mixture, Phys. Rev. E **55**, 6624 (1997).

[56] N. B. Wilding and F. Schmid, Wetting of a symmetrical binary fluid mixture on a wall, Comp. Phys. Comm. **147**, 149 (2002).

[57] F. Schmid and N. B. Wilding, Wetting of a symmetrical binary fluid mixture on a wall, Phys. Rev. E **63**, 031201 (2001).

[58] N. B. Wilding, Continuous demixing at liquid-vapor coexistence in a symmetrical binary fluid mixture, Phys. Rev. E **67**, 052503 (2003).

[59] N. B. Wilding, F. Schmid, and P. Nielaba, Liquid-vapor phase behavior of a symmetrical binary fluid mixture, Phys. Rev. E **58**, 2201 (1998).

[60] J. Köfinger, G. Kahl, and N. B. Wilding, Phase behaviour of a symmetrical binary mixture in a field, Europhys. Lett. **75**, 234 (2006).

[61] J. Köfinger, G. Kahl, and N. B. Wilding, Phase behavior of a symmetrical binary fluid mixture, J. Chem. Phys. **125**, 234503 (2006).

[62] W. Kob and H. C. Andersen, Scaling behavior in the β-relaxation regime of a supercooled Lennard-Jones mixture, Phys. Rev. Lett. **73**, 1376 (1994).

[63] W. Kob and H. C. Andersen, Testing mode-coupling theory for a supercooled binary Lennard-Jones mixture: The van Hove correlation function, Phys. Rev. E **51**, 4626 (1995).

[64] U. R. Pedersen, T. B. Schrøder, and J. C. Dyre, Phase diagram of Kob-Andersen-type binary Lennard-Jones mixtures, Phys. Rev. Lett. **120**, 165501 (2018).

[65] C. P. Royall and W. Kob, Locally favoured structures and dynamic length scales in a simple glass-former, J. Stat. Mech. 024001 (2017).

[66] F. Turci, C. P. Royall, and T. Speck, Devitrification of the Kob-Andersen glass former: Competition with the locally favored structure, J. Phys.: Conf. Ser. **1252**, 012012 (2019).

[67] T. S. Ingebrigtsen, J. C. Dyre, T. B. Schrøder, and C. P. Royall, Crystallization instability in glass-forming mixtures, Phys. Rev. X **9**, 031016 (2019).

[68] C. Luo, J. F. Robinson, I. Pihlajamaa, V. E. Debets, C. P. Royall, and L. M. C. Janssen, Many-body correlations are non-negligible in both fragile and strong glassformers, Phys. Rev. Lett. **129**, 145501 (2022).

[69] F. Leoni, F. Martelli, C. P. Royall, and J. Russo, Structural signatures of ultrastability in a deposited glass-former, Phys. Rev. Lett. **130**, 198201 (2023).

[70] S. Mehri, T. S. Ingebrigtsen. and J. C. Dyre, Single-parameter aging in a binary Lennard-Jones system, J. Chem. Phys. **154**, 094504 (2021).

[71] M. Schmidt, Power functional theory for many-body dynamics, Rev. Mod. Phys. **94**, 015007 (2022).

[72] F. Sammüller and M. Schmidt, Adaptive Brownian dynamics, J. Chem. Phys. **155**, 134107 (2021); (Selected as Featured, Coverpage).

[73] R. Evans, J. R. Henderson, D. C. Hoyle, A. O. Parry, and Z. A. Sabeur, Asymptotic decay of liquid structure: oscillatory liquid-vapour density profiles and the Fisher-Widom line, Mol. Phys. **80**, 755 (1993).

[74] R. Evans, R. J. F. Leote de Carvalho, J. R. Henderson, and D. C. Hoyle, Asymptotic decay of correlations in liquids and their mixtures, J. Chem. Phys. **100**, 591 (1994).

[75] M. Dijkstra and R. Evans, A simulation study of the decay of the pair correlation function in simple fluids, J. Chem. Phys. **112**, 1449 (2000).

[76] C. Grodon, M. Dijkstra, R. Evans, and R. Roth, Decay of correlation functions in hard-sphere mixtures: Structural crossover, J. Chem. Phys. **121**, 7869 (2004).

[77] V. Molinero and E. B. Moore, Water modeled as an intermediate element between carbon and silicon, J. Phys. Chem. B **113**, 4008 (2009).

[78] S. Saw, N. L. Ellegaard, W. Kob, and S. Sastry, Structural relaxation of a gel modeled by three body interactions, Phys. Rev. Lett. **103**, 248305 (2009).

[79] S. Saw, N. L. Ellegaard, W. Kob, and S. Sastry, Computer simulation study of the phase behavior and structural relaxation in a gel-former modeled by three-body interactions, J. Chem. Phys. **134**, 164506 (2011).

[80] F. Sammüller, D. de las Heras, and M. Schmidt, Inhomogeneous steady shear dynamics of a three-body colloidal gel former, J. Chem. Phys. **158**, 054908 (2023). (Special Topic on Colloidal Gels).

[81] F. H. Stillinger and T. A. Weber, Computer simulation of local order in condensed phases of silicon, Phys. Rev. B **31**, 5262 (1985).

[82] D. Frenkel and B. Smit, *Understanding Molecular Simulation: From Algorithms to Applications,* 3rd ed. (Academic Press, London, 2023).

[83] N. B. Wilding, Computer simulation of fluid phase transitions, Am. J. Phys. **69**, 1147 (2001).

[84] A. V. Brukhno, J. Grant, T. L. Underwood, K. Stratford, S. C. Parker, J. A. Purton, and N. B. Wilding, DL_MONTE: a multipurpose code for Monte Carlo simulation, Molec. Simul. **47**, 131 (2021).

[85] T. Eckert, N. C. X. Stuhlmüller, F. Sammüller, and M. Schmidt, Fluctuation profiles in inhomogeneous fluids, Phys. Rev. Lett. **125**, 268004 (2020).

[86] T. Eckert, N. C. X. Stuhlmüller, F. Sammüller, and M. Schmidt, Local measures of fluctuations in inhomogeneous liquids: Statistical mechanics and illustrative applications, J. Phys.: Condens. Matter **35**, 425102 (2023).

[87] M. K. Coe, R. Evans, and N. B. Wilding, Measures of fluctuations for a liquid near critical drying, Phys. Rev. E **105**, 044801 (2022).

[88] M. C. Stewart and R. Evans, Phase behavior and structure of a fluid confined between competing (solvophobic and solvophilic) walls, Phys. Rev. E **86**, 031601 (2012).

[89] R. Evans and M. C. Stewart, The local compressibility of liquids near non-adsorbing substrates: a useful measure of solvophobicity and hydrophobicity?, J. Phys.: Condens. Matter **27**, 194111 (2015).

[90] R. Evans, M. C. Stewart, and N. B. Wilding, A unified description of hydrophilic and superhydrophobic surfaces in terms of the wetting and drying transitions of liquids, Proc. Natl. Acad. Sci. **116**, 23901 (2019).

[91] M. K. Coe, R. Evans, and N. B. Wilding, Density depletion and enhanced fluctuations in water near hydrophobic solutes: identifying the underlying physics, Phys. Rev. Lett. **128**, 045501 (2022).

[92] D. Borgis, R. Assaraf, B. Rotenberg, and R. Vuilleumier, Computation of pair distribution functions and three-dimensional densities with a reduced variance principle, Mol. Phys. **111**, 3486 (2013).

[93] D. de las Heras and M. Schmidt, Better than counting: Density profiles from force sampling, Phys. Rev. Lett. **120**, 218001 (2018).

[94] B. Rotenberg, Use the force! Reduced variance estimators for densities, radial distribution functions, and local mobilities in molecular simulations, J. Chem. Phys. **153**, 150902 (2020).

[95] S. W. Coles, E. Mangaud, D. Frenkel, and B. Rotenberg, Reduced variance analysis of molecular dynamics simulations by linear combination of estimators, J. Chem. Phys. **154**, 191101 (2021).

[96] A. J. Schultz, S. G. Moustafa, W. Lin, S. J. Weinstein, and D. A. Kofke, Reformulation of ensemble averages via coordinate mapping, J. Chem. Theory Comput. **12**, 1491 (2016).

[97] A. Purohit, A. J. Schultz, and D. A. Kofke, Force-sampling methods for density distributions as instances of mapped averaging, Mol. Phys. **117**, 2822 (2019).

[98] S. G. Moustafa, A. J. Schultz, D. A. Kofke, Reformulation of expressions for thermoelastic properties of crystals using harmonic mapping, Phys. Rev. B **106**, 104105 (2022).

[99] N. D. Mermin, Thermal properties of the inhomogeneous electron gas, Phys. Rev. **137**, A1441 (1965).

[100] Simulation data will be openly available at: doi.org/10.5281/zenodo.17041037.